ELSEVIER

Near-IR bromine Laser Induced Breakdown Spectroscopy detection and ambient gas effects on emission line asymmetric Stark broadening and shift

George Asimellis [a,*], Aggelos Giannoudakos [b,c], Michael Kompitsas [c]

[a] Aristotle University of Thessaloniki, Faculty of Physics, Thessaloniki 54124, Greece
[b] School of Chemical Engineering, National Technical University of Athens, 9, Iroon Polytechniou Street, Zografou, 15780 Athens, Greece
[c] National Hellenic Research Foundation, Theoretical and Physical Chemistry Institute, 48 Vasileos Konstantinou Avenue, 11635 Athens, Greece

Abstract

Investigation via Laser-Induced Breakdown Spectroscopy of a near-infrared bromine emission line (827.2 nm) with an UltraViolet ablation laser and a gated detector is reported. The effects of ambient pressure and gas species (air, O_2, N_2 and He) on the atomic emission line strength and spectral profile were systematically investigated. Substantially improved signal strength and reduced background radiation are demonstrated near 100 mbar ambient pressure with all gases. Optimal results were achieved when helium was used. Asymmetric broadening and shift of the 827.2 nm bromine line, attributed to pressure-dependent Stark effect has been revealed. This effect is prominent when air, oxygen or nitrogen are present and is much less manifested when helium is used. Possible interpretations of this effect are presented.
© 2006 Published by Elsevier B.V.

Keywords: Laser-induced breakdown spectroscopy; Halogen detection; Bromine content; Stark effect; Ambient gas effects

1. Introduction

Laser ablation, excitation, followed by ionization and detection of atomic relaxation radiation from the laser-induced plasma is the basis of Laser-Induced Breakdown Spectroscopy (LIBS), also called Laser-Induced Plasma Spectroscopy (LIPS).

The experimental realization of LIBS is simple: a short-duration laser pulse is focused on the sample, vaporizing a small amount. Via further photon (and multi-photon) absorption, atoms and ions are created in a hot (many 1000 K) plasma. After ion–electron recombination, subsequent radiative decay leads to emission of atomic lines. This signal is spectroscopically analyzed and thus the sample elemental composition can be identified. As a rule, time-resolved (gated) detection is employed to differentiate between specific emission lines. The majority of LIBS applications still deal mainly with metallic elements. However, elements with strong non-metallic character, such as sulfur, carbon and phosphorus, as well as the halogens, have been less investigated. It must be emphasized though, that efficient qualitative and quantitative determination of these high-excitation energy, non-metallic elements is necessary in a wide range of applications, such as: analysis of pharmaceutical products (chlorine and fluorine), on-line compositional analysis of molten metals and alloys (carbon, silicon, phosphorus etc.), trace element detection in hazardous gases, aqueous solutions, and chemical weapons (chlorine and fluorine), environmental applications (sulfur), mineral classification and ore beneficiation (phosphorus), electronics recycling (bromine), etc. The fact that non-metallic elements have not been thoroughly investigated by LIBS can be attributed to that, due to their energy-level distributions, their strongest atomic emission lines lie in the Vacuum UltraViolet (VUV, 125–190 nm) [1]. Practical application of LIBS in this range is complicated by strong atmospheric oxygen absorption (requiring a vacuum, or at least oxygen-free light path), the lack of stable, gated (iCCD) detectors with adequate sensitivity, and the need to use expensive non-UV-absorbing (such as MgF_2- or CaF_2-based) optics, since non-fused SiO_2 strongly absorbs in the UV. In addition, spectrometers for this region are not fully effective, neither are simple and convenient.

Most non-metallic elements exhibit also visible and Near InfraRed (NIR, 700–900 nm) [2,3] emission lines, but less strong than those in the VUV. The visible lines correspond to

* Corresponding author.
E-mail address: gasim@auth.gr (G. Asimellis).

transitions between short-lived ionic excited states. Short delays and long accumulations are required for observation of these lines, hindering detection. The NIR lines correspond to transitions between atomic excited states, and thus they are more suitable for LIBS detection. Compared to VUV, detection in the NIR offers several advantages, namely: use of regular SiO_2-based fibers and conventional optics for imaging, no need for vacuum or oxygen-free light path, i.e. operation can be achieved under atmospheric conditions, etc. Recently, halogens (F [4–6], Cl [7,8], Br [9]), as well as S [10–12], have been detected in the VUV or in the NIR via LIBS. Bromine ionic emission lines were detected also in the 470 nm [6]. Initial reports in the VUV and NIR show generally weak signal strength and poor signal- to-ratio because of a very strong background (electron deceleration) radiation. All these experiments employed an IR ablation laser, and for detection either a non-gated detector, or a gated one with poor NIR sensitivity. When an inert gas was used, gas flow or diluted inert gas techniques have been used. In all studies, plasma was formed under atmospheric pressure.

1.1. Motivation for bromine LIBS detection

Bromine detection is important in a wide array of applications, ranging from the coal Industry [13 14], waste combustion and material recycling [15] to environmental applications. Bromine's natural concentration (less than 50, rarely up to 200 mg/kg) is significantly lower than of other halogens, such as chlorine. However, increased Br concentrations are present in some industrial products, such as flame-retarded foams, textiles and plastics, products increasingly used in automobiles and in the electrical and electronic industry.

Heat-insulating foams such as polyurethane (PUR), expanded (XPS) and extruded (EPS) polystyrene, contain hexabromocyclododecane (HBCD). When such waste is disposed of by thermal treatment/combustion, the influence of bromine on the combustion process needs to be considered due to its adverse effect on fly ash and stack emissions, as shown by studies on bromine content in combustion waste from coal-fired thermoelectric power stations [16]. In addition, in such heat-insulating materials, brominated compounds are accompanied by synergist mixes to increase flame retardant efficiency (e.g. antimony trioxide [17], thermal and photochemical stabilizers). Typical dosage is one part of Sb_2O_3 to two parts of the bromine compound. Thus monitoring bromine levels aids antimony detection. The bromine-containing polymeric materials in electrical and electronic modules such as polybrominated biphenyl (PBB), polybrominated diphenyloxide (PBDPO), or tetrabromobisphenol-A (TBBPA) can contain Br concentrations of 4 wt.% or more. TBBPA is used as a parent compound for other flame retardants, such as TBBPA-bis 2-hydroxyethyl ether,-dibromopropylether,-bis allylether,-carbonate oligomer and brominated epoxy oligomer. These compounds must be identified and eliminated due to their potential health hazard [18,19], responsible for dermatitis, chronic bronchitis and asthma, neurological damage, adverse effects of the liver, kidney, and hematopoietic

systems. PBBs and PBDPOs are reported in at least 9 of the 1647 National Priorities Lists identified by the US Environmental Protection Agency (EPA).

Other bromine-related environmental applications include solvent-based paints and gaseous compounds, such as HBr, which forms strong acidic aqueous solutions and affects ozone layer depletion. During peak periods of ozone events, average atmospheric concentration of Br can reach 130 ppt, while 'normal' levels are up to 15 ppt [20]. The so-called 'filterable' bromine (mostly inorganic bromine Br), has been found to adversely affect ozone depletion [21]. Bromine is present in seawater to approximately 60 ppm, but has been found in much higher concentrations in the thalli of some red algae [22] and thus its determination in marine algae has raised some interest [23].

2. Experimental

2.1. Most important experimental steps

In two recent publications we reported qualitative and quantitative NIR LIBS determination of fluorine at 685 nm, chlorine at 835 nm [24], and sulfur [25] at 869 nm. Improved signal detection metrics, such as signal-to-noise ratio, reduction of the limit of detection (LOD) and good calibration linearity was demonstrated. These results reflect the combined benefits of the experimental steps taken. In the present work, we applied this technique for an efficient LIBS bromine determination in the NIR. The most important experimental steps in our work are the following:

- An intensified, gated sensor with improved spectral response in the NIR was used for detection. This is the new-generation Andor Technology GEN III *i*CCD [26], which enables time-resolution with near-constant quantum efficiency (Q.E. $\approx$ 20%) from 600 to 900 nm. Plasma radiation is emitted by many mechanisms, such as electron deceleration (*Bremsstrahlung*) radiation, followed by atomic bound—bound emission due to relaxation. Thus as the plasma gradually cools, the atomic emission lines of interest appear after the initial broad-band radiation. Different atomic emission lines appear at different times, within the lifetime (up to 20 μs) of plasma duration. By optimizing gate delay (time elapsed after laser firing) and width (duration of collection), discrimination in favor of specific lines of interest was possible.
- Contrary to most previous halogen detection reports employing an IR ablation laser (e.g. Nd:YAG fundamental, 1.064 μm), a UV laser (Nd:YAG operating at its third harmonic 0.355 μm) was employed in our work. Use of the tripled laser frequency was aiming to improve energy coupling onto the sample (energy transfer onto the sample leading to enhanced material evaporation), enhance plasma ionization/excitation and reduce plasma-shielding effects (leading to improved atomic optical emission). When using an IR laser, absorption is mainly due to multi-photon, rather than single-photon (radiation below-1-μm may cause multi-
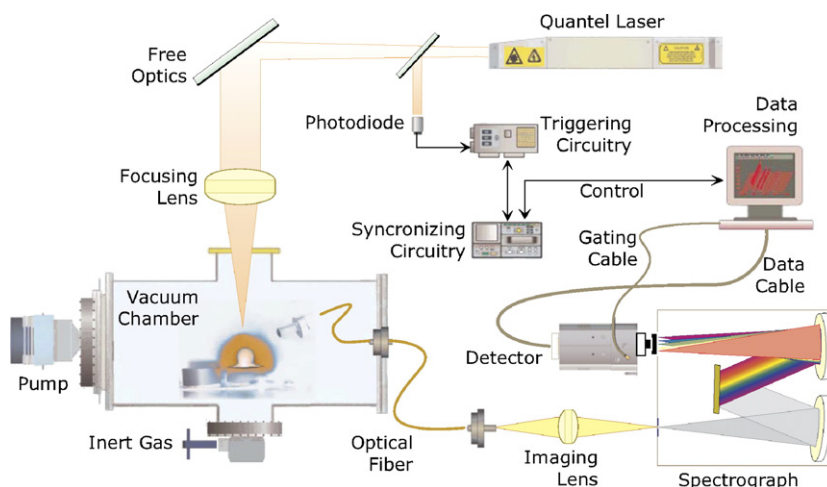
Fig. 1. Schematic of the experimental setup.

photon absorption too, yet to a lesser degree than the above-1-μm radiation). On the contrary, a UV laser, being better coupled onto the sample, is more effective for ablation and for plasma ionization/excitation.

More important is the subsequent inhibition of the laser pulse energy transfer to the sample and the plasma particles. As the plasma is formed, its electron density n_e, and thus its plasma frequency (ω_p, proportional to the square root of electron density, n_e) are increasing. As soon as ω_p becomes larger than the laser frequency, the plasma starts to reflect the laser radiation (plasma shielding [27–30]), becoming opaque. Thus little of the remaining laser energy participates in the evaporation and ionization processes. A UV laser is more effective on penetrating the plasma and subsequently producing an analyte-richer plasma. Depending on laser pulse energy, studies have shown that while plasma reflectivity with a UV laser is in the order of 20%, for an IR is reduced to just 7%. For example, with a XeCl laser (308 nm), the 'threshold' for plasma shielding is in the order of sub GW per pulse [31]. Our pulse energies were far below this mark.

- While all previous halogen detection was performed either at atmospheric conditions with gas flow or dilution techniques [32], plasma in this series of experiments was formed in a vacuum chamber under various ambient gases (He, N_2, O_2, and air), with precisely-controlled pressure from a few mbar to 1 atm. It is known that plasma evolution and emission properties depend heavily on (*a*) the ambient pressure and (*b*) the ambient species. A reduced ambient pressure favors plasma expansion and reduces electron breaking radiation (background noise). In addition, if instead of air (nitrogen or oxygen) an inert ambient gas (argon or helium) is used, the optical emission line strength is significantly improved [7]. By using various gases and precisely controlling ambient pressure, the effect of ambient gas pressure and species (type) on bromine emission signal strength was systematically investigated. It is emphasized that controlled inert gas pressure cannot be achieved with previously-reported gas flow or dilution techniques.

2.2. Experimental details

As shown in Fig. 1, excitation was provided by a Q-switched pulsed Nd:YAG laser (Quantel YG 981), operating on its third harmonic, with pulse duration of 9 ns and pulse energy ranging from 10 to 26 mJ per pulse, operating at 5 Hz. The laser beam was delivered to the sample by free-path optics, leading to a converging quartz lens (f = 150 mm), which focused the beam just below ($\approx$ 1 mm) the sample surface. A fast photodiode (rise time 1 ns) responding to the laser pulse via a beam splitter provided the triggering signal. Optical emission was collected by a 2 m long quartz optical fiber located close to the plasma (CVI Laser Corp., core $\varnothing$ 0.4 mm, numerical aperture (N.A.) 0.22). The fiber exit was directed on the entrance slit of a Jobin-Yvon HRP Czerny-Turner type spectrometer (1 200 lines/mm grating, 600 mm focal length, 80 to 200 μm entrance slit width). To ensure that only first-order diffraction spectra were recorded, a 0.5 μm cut-off filter was placed in front of the spectrometer entrance slit.

Plasma was formed in a tailored-built vacuum chamber, in which the ambient gas pressure could be accurately controlled with a below-mbar precision fine-metering valve and measured by a MKS Baratron gauge. Samples were placed on a X–Y translator, driven by PC-controlled stepper motors. Relative target position versus the incident laser beam was changed every 5 pulses at a step of 0.5 mm: an area of about 5 × 5 mm was scanned each time. Thus, possible inhomogeneity and pitting effects were reduced and data were more representative of the sample concentration.

Time-resolved measurements were performed with an Andor iStar DH734-18F-73 Gen III filmless gated iCCD detector, (1024 × 256 pixel-wide active sensor). The extent of the sensor corresponded to approximately 20 nm, dictated by the grating dispersion function and the detector sensitive area (18 mm for 1024 pixels). The detector was triggered externally. Gate delay values from 100 ns to 1 μs and gate widths from 10 to 20 μs were used. The best possible gain and gate values were experimentally determined to optimize signal-to-noise. For every new sample, first the real-time mode was used to optimize signal, by selecting gain,

width and delay via the camera's user interface (Andor iStar 3.2). Subsequently, the accumulation mode was selected, collecting from 50 up to 200 spectra each time. Data were then processed by standard software (Microcal Origin™ 6.0).

To perform initial wavelength calibration and peak assignment, the Ne emission spectrum from a Na hollow cathode (HC) lamp was recorded, using wavelength values from [33]. This spectrum calibration was aided by the wavelength calibration technique reported in Ref. [34], and as a result, across the 1024-pixel wide axis, a wavelength accuracy of 0.5 Å or better was achieved.

A series of reference samples were prepared by mixing chemically pure KBr and K_2CO_3 powders. Sample preparation involved microbalance weighting, mortar and pestle mixing, grounding and homogenization, and then high-pressure processing (10 atm for 5 min) of 1 g mix to produce 13 mm $\varnothing$, $\approx$ 4 mm thick tablets with decreasing bromine concentrations from 33.6 wt.% to 1 wt.% (wt.%=mg/kg×10^{-4}). Pure K_2CO_3 samples were used as reference to aid definite Br lines determination.

3. Results and discussion

3.1. Bromine spectra and line assignments

Br (I) NIR spectrum includes, in decreasing order of intensity, the 827.24 nm, 882.5 nm, 889.8 nm, and 926.5 nm major emission lines. We therefore chose to investigate the 827 nm region. For line assignment, three spectra were recorded (plotted in Fig. 2, vertically separated, for clarity). The top spectrum represents the Na HC emission spectrum, followed by two LIBS spectra: the middle spectrum corresponds to a pure K_2CO_3 tablet in 70 mbar N_2 ambient gas and, finally, the bottom spectrum corresponds to a chemically pure KBr tablet (to reveal the Br lines) in 70 mbar He. All LIBS spectra correspond to 100 accumulations, with 1 μs delay and 20 μs width, and a gain of 86 on the 0 to 255 scale.
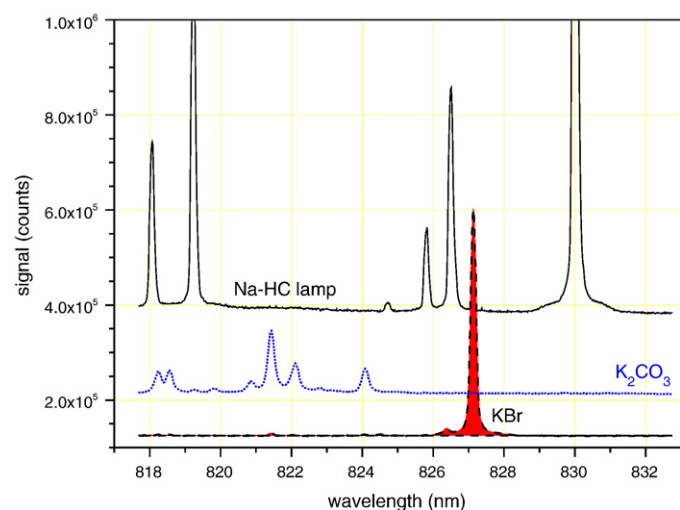

Fig. 2. Line assignment for spectra in the 818–830 nm window. The top represents Na HC spectrum, the middle, K_2CO_3 spectrum, and the bottom represents KBr spectrum. The LIBS spectra were recorded for 1 and 20 μs gate delay and width, respectively.
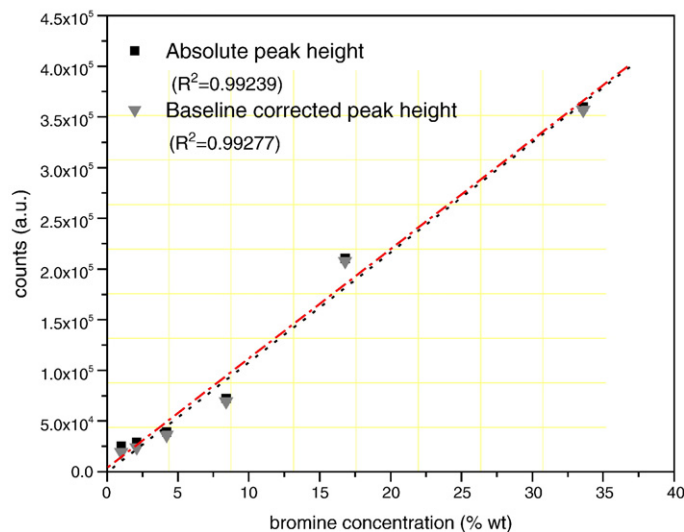

Fig. 3. Calibration curve of bromine for the net bromine signal from KBr+ K_2CO_3 samples in 30 mbar He ambient gas pressure. Signal strength was derived from the bromine 827.24 nm line.

From the HC spectrum, the two lines at 818.07 and 819.32 nm are assigned as Na emissions; all other lines are assigned as Ne emissions. From the KBr spectrum, the weak 826.50 nm and the strong 827.24 nm line appear fully resolvable. Their relative strength appears to be in accordance with their corresponding coefficients of the order of 1:10 [33]. The K_2CO_3 spectrum has neither of these two bromine lines, as expected.

The KBr spectrum has a significantly improved interference-free line profile, with drastically reduced background level (noise). It is clear that a considerable improvement of the Br optical emission signal has been achieved. The 827.24 nm Br line in the KBr spectrum can be compared with that of Fig. 7a of Ref. [9], a very recent NIR LIBS Br investigation. Good signal-to-ratio and large photon-count measurements enable enhanced detection robustness and reduced limit of detection (increased sensitivity).

3.2. Concentration calibration curves

The most-frequently used method for concentration calibration curves in LIBS is the internal standardization (IS). The conditions for the applicability and the details of this method are described in Refs. [24] and [35]. Briefly, the line intensity ratio of two elements, an analyte and a reference, is plotted against the known elemental concentrations in a series of reference samples. Under the same experimental conditions, a good calibration curve linearity is expected.

However, if there is no presence of a reference spectral line, application of the IS method is not possible. This is the case with the KBr spectrum: only bromine lines are present (Fig. 2) when helium (at 30 mbar) was used, and all other lines, except for the Br 827.24 nm line stem from the ambient gas (nitrogen or oxygen at 800 mbar), Fig. 4. Therefore, the absolute bromine signal strength (peak-to-baseline) was selected as metric. The absolute Br line strength, measured in a number of different ways, is plotted in Fig. 3 against the sample's bromine concentration in each of the prepared samples. Data used correspond to helium at
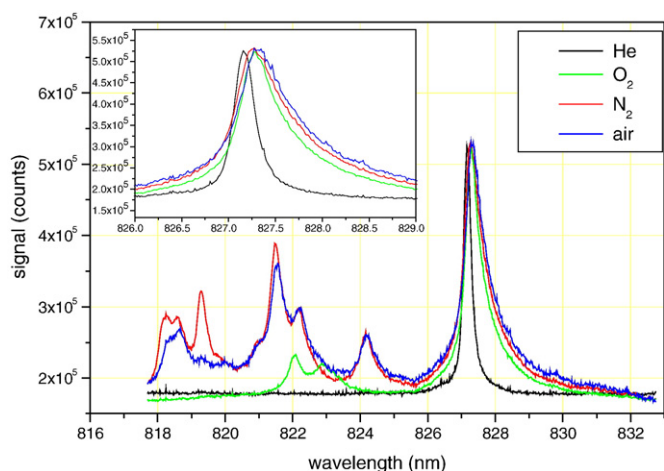
Fig. 4. Bromine emission in the 827 nm range for 100 accumulations. Ambient gas was 800 mbar for the all gases used. Gate delay and width were the same as for Fig. 2.

30 mbar and a 26 mJ per pulse laser energy. In all cases, the calibration curve linearity (expressed by the coefficient of determination, R) is quite satisfactory. The present lowest detectable values can be further reduced, by improving light collection efficiency (e.g. by using a lens or mirror to collect light from a larger plasma volume, using a fiber with larger core diameter and N.A., etc.).

3.3. Ambient gas pressure dependence of bromine emission line strength

In addition to He, KBr emission spectra were separately recorded with air, nitrogen and oxygen as ambient gas, shown in comparison with the He spectra in Fig. 4. All experimental parameters were the same as those in Fig. 2, except that the ambient gas pressure was set at 800 mbar, the highest value used in this series of measurements. The spectra have been normalized with respect to the bromine line in He ambient gas. None of the broad peaks in the 818–826 nm range, due to nitrogen and oxygen, interferes with the 827.24 nm bromine line. However, a shift and an asymmetric broadening of the bromine line is observed (see inlet in Fig. 4), depending significantly on the kind of ambient gas. Not only the Br 826.50 nm line disappears into the blue wing of the 827.24 nm Br line, but also this broadening decreases line discrimination and clarity that can possibly interfere with other lines in practical applications with adverse effects on detection ability. This effect though is much less manifested when He is used.

To investigate the effect of gas pressure on emission signal strength, spectra with varying pressure from near vacuum (10^{-2} mbar) to 800 mbar were recorded. We initially used He, and studied the effect of ambient pressure on the bromine 827.24 nm line strength. A drastic increase of the signal strength between vacuum to about 100 mbar was observed. Beyond 100 mbar, as pressure increased, line strength decreased significantly. There appears to be an optimum He pressure in the range of 60–100 mbar, for which the emission signal is maximized. Comparable behavior was also shown in our previous

investigations under similar conditions for fluorine, chlorine [24], and sulfur [25]. This behavior is attributed to:

- A drastic background (*Bremsstrahlung*) radiation reduction, due to the significantly reduced 'breaking power' of the surrounding environment, allowing plasma to expand optimally. In agreement with recent reports [36,37], emission lines produced under low pressure appeared sharper than those produced under atmospheric or higher pressure. Of course, there is a 'sweet spot' (in the range of 60–100 mbar), since in near-vacuum plasma expands too fast to reach a certain volume and temperature.

- By the non-participation of the ambient gas in plasma charge population. An inert gas, having a very high ionization potential (IP), such as He at 24.6 eV, is not — to a large degree — ionized, and thus neither absorbs laser energy, nor contributes to unnecessary charge population in the plasma. (As much as a rich ion population emanating from the sample is desired, additional charge population emanating from the ambient environment only increases plasma frequency.) Thus, with an inert gas ambient environment the ions in the plasma originate mainly from the sample and there is no further contribution to the plasma frequency.

When using N_2, O_2, and air as ambient gas, a similar trend was demonstrated. Therefore, it is expected that similar mechanisms, as discussed above, affect the bromine signal pressure dependence. Some differences were observed when N_2 was used: first, peak maximum appeared at a lower pressure ($\approx$ 30 mbar) than for the other gases. This is strongly correlated with a steeper increase of the signal in the "low" pressure range. Second, the bromine emission signal drops faster in the "high" pressure range, reaching a low plateau for pressures higher than 300 mbar. I.e., when using N_2, the bromine signal pressure dependence appeared "narrower" than for the other gases, and the maximum signal more sensitive on the value of ambient pressure.

When using atmospheric air, the pressure dependence of the bromine signal (Fig. 5) is the combined effect of the pressure
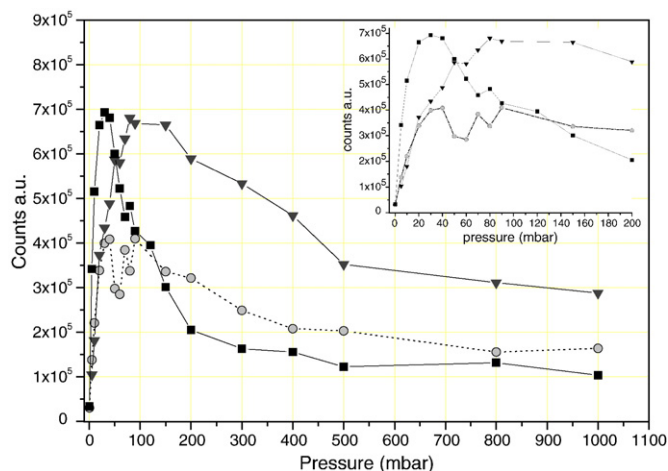

Fig. 5. Dependence of the bromine 827.24 nm line of a KBr sample on the ambient gas pressure for 1 µs delay and 20 µs width of the time window, for N_2 (■), O_2 (▼) and air (○). (1 mbar corresponds to 100 Pa).
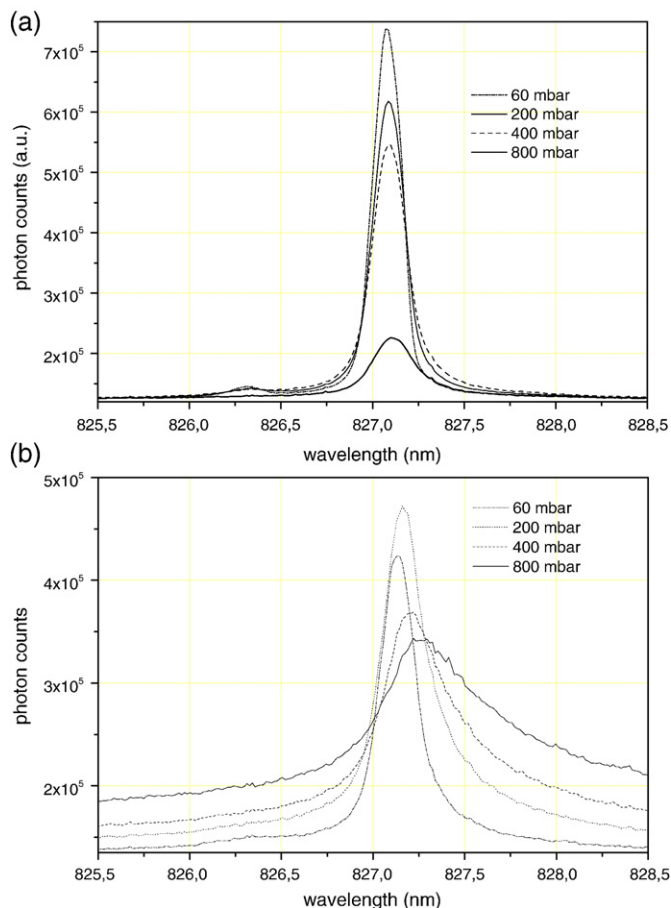
Fig. 6. Dependence of the Br 827.24 nm line profile for 60, 200, 400 and 800 mbar (a) in He ambient and (b) in air ambient gas. Delay and width of the observation window was 1 and 20 μs respectively.

dependence of N_2 and O_2. Considering that the ratio of N_2 to O_2 in atmosphere is 4:1, the fast initial rise of the bromine signal follows the fast increase observed for when just N_2 was used. In the "high" pressure range, the O_2 contribution dominates in the atmosphere-dependent signal. The signal strengths of the three curves in the 0 to 200 mbar pressure range (including the maximum of the three curves) are shown in the inlet, Fig. 5.

Similar pressure dependence of the emission signal in LIBS experiments has been reported under atmosphere and other noble gases. It has been found that argon, for example, maximizes emission signal at about 140 mbar [38], while the maximum for atmospheric air appears at 300 mbar. While there is a general agreement, there are differences in the optimal pressure value, as well as in the rate of the signal increase/decrease in the "low" and "high" pressure ranges. In the present experiment, the bromine signal maximum occurs at a lower N_2 pressure than for all other gases studied. This suggests that plasma shielding inaugurates at a lower N_2 pressure, compared to the other gases. An explanation for this would be that N_2 tends to ionize easier than O_2 and a denser plasma builds up at a lower pressure. From the point of view of the IP values for the two gases (15.58 eV for N_2 and 12.06 eV for O_2) alone, this is rather a discrepancy. Therefore, some other mechanism, related to another physical property of the two gases must be considered. This might not be independent

on the experimental parameters used in this series of measurements, such as the observation window (1 μs gate delay and 20 μs width). To fully investigate the effect, a more systematic investigation is required and in particular, separate measurements on the signal, background (stemming from the ambient gas), and signal-to-noise ratio has to be performed.

3.4. Shift and asymmetric broadening of the 827.24 nm bromine line

As it has been indicated in Section 3.3, an asymmetric broadening and shift of the 827.24 nm bromine peak (Figs. 4 and 6) is clearly demonstrated for all gases used. Based on the observations made on Fig. 4, we systematically investigated the 827 nm bromine line profile dependence of the pressure for He, N_2, O_2, and atmospheric air, in the pressure range from a few mbar to 800 mbar. The results are plotted for the two selected cases, for He in Fig. 6a, and atmospheric air in Fig. 6b. For clarity, only four spectra for both ambient gases, corresponding to increasing pressure 60, 200, 400, and 800 mbar, are shown. Gate delay and width were the same as those used in Fig. 4. We observe for He a very limited shift and broadening even for the highest (800 mbar) pressure used. On the contrary, line shift and broadening under atmospheric air is much larger. Tabulated results reporting FWHM broadening $\Delta\lambda_{1/2}$ (nm), and line shift, $\Delta\lambda_{shift}$ (nm) are reported in Table 1 for four different pressure values. Reported line shift is measured from the 60 mbar line profile, which is used as a reference. In summary:

- There is an undisputable shift and asymmetric broadening observed with all gases used. The extent of shift and broadening depends on the gas species used. Helium manifests the least shift and broadening.
- The effect is dependent on ambient pressure. With increasing pressure, both shift and broadening increase with an almost linear fashion.

The explanation for such line shift and broadening is the Stark or electrochromic effect [39], the perturbation resulting from interaction between an excited radiating state and a strong external electric field stemming from charged particles, such as electrons and ions. The resulting shift and broadening is dependent on the external electric field, and thus to the ion and electron densities. Laser-induced plasmas are likely to exhibit

Table 1
FWHM broadening $\Delta\lambda_{1/2}$ (nm), and line shift, $\Delta\lambda_{shift}$ (nm) for four different pressure values for He and atmospheric air

He			Atmospheric air	
Pressure	Shift	Broadening	Shift	Broadening
mbar	nm	nm	nm	nm
80	–	0.100	–	0.250
200	0.008	0.148	0.025	0.313
400	0.011	0.203	0.068	0.500
800	0.029	0.324	0.150	0.813

Line shift is measured from the 60 mbar data.

such an effect, given their high electron and ion densities. [40]. Not all radiating states can manifest Stark effect, however: the effect is related to the degree of degeneracy of the radiating state [41]. For example, states with higher principle quantum number are likely to display a larger shift and broadening for a given ion and electron density.

In high electron density plasmas, neutral atoms (other than H) are mostly influenced by the quadratic Stark effect due to electrons, and the weaker ionic influence is often neglected. The formulas for FWHM linewidth, $\Delta\lambda_{1/2}$ (Å), and line shift, $\Delta\lambda_{shift}$ (Å) are [42–44]:

$$\Delta\lambda_{1/2} = \{2 + 5.53 \times 10^{-6} n_e^{1/4} A(1-0.0068 n_e^{1/6} T_e^{-1/2})\} \times 10^{-22} w_e n_e \qquad (1)$$

$$\Delta\lambda_{shift} = \{(d/w_e) + 6.32 \times 10^{-6} n_e^{1/4} A(1-0.0068 n_e^{1/6} T_e^{-1/2})\} \times 10^{-22} w_e n_e \qquad (2)$$

where n_e (m^{-3}) is the electron number density, T_e (K) the plasma absolute temperature, w_e (m) and A (m) the electron and ion broadening (impact width) parameters, respectively, both weak functions of temperature, and d/w_e (dimensionless) the ratio of shift to width.

Some remarks on the above formulae:

- Since plasma temperature and electron density are rapidly changing within ns intervals, line broadening ($\Delta\lambda_{1/2}$) and shift ($\Delta\lambda_{shift}$) are highly dependent on time.
- If electron-only interaction is considered ($A=0$) [45], a symmetric line broadening is expected. Symmetrically broadened and shifted line profiles (electron-only interaction) have been often observed in laser-produced plasmas, and
- When an asymmetric broadening is observed, there is strong indication that there is a non-trivial ionic influence.

The remaining question is: why is the observed profile asymmetric? There are two possible explanations:

a) The asymmetry is due to the Stark ionic interaction with the excited bromine state. The observed asymmetry towards lower energies supports this. All curves in Fig. 4 correspond to the same integration time (20 μs), but the line profile under helium demonstrates a very limited shift and broadening. The fact that the least dependence of line shift and broadening on ambient pressure is manifested for helium (i.e. highest IP) suggests that the ionic effect is due to ions emanating from the ambient environment. Under the very same conditions, the dependence of line shift and asymmetric broadening on ambient pressure with air (Fig. 6b) is substantially larger. There is good indication that there is a prerequisite that for this effect to be manifested at all, namely that specific energy-level distribution involved with the atomic transition must exist. Ambient gas pressure measurements performed by our group for F and Cl [24] and S [25] in He ambient gas for the same pressure range and similar gate

width parameters did not produce any indication for an asymmetric broadening and shift, even for the highest pressure values used. Similarly, in Fe I LIBS spectra in air [35] using both the IR (fundamental) and the third harmonic (355 nm) of a Nd:YAG, no observation of a shift or asymmetric line broadening was recorded. Observation of spectral data shown in Fig. 2 of Ref. [46], supports that the manifestation of ionic effects is related with the energy levels involved with the specific atomic transition: under the same experimental parameters (such as gate width), a red- or blue-asymmetric shifts (or even unaffected lines) can be observed.

b) Our present experimental findings were obtained with a relatively large gate width, and thus were more representative of a space- and time-average result of a highly dynamical evolution of both electron and ion number densities. It is very likely that the observed profile represents an overlap of several different profiles, each characterized by a different — possibly symmetric — Stark broadening and shift, experienced during the duration of observation, each characterized by a different Stark broadening and shift. These profiles can be considered — to a first approximation — as corresponding to an increasing delay and constant width (e.g. if each has 1 μs delay and 1 μs width, the n-th contribution has $n+1$ μs delay and 1 μs width). Because charge number densities and temperature decrease drastically with time, each contribution has a different Stark shift and broadening. For increasing delay, the corresponding line shift and broadening, as well as the photon count per contribution, decrease. Combined together, they produce an asymmetric and shifted profile.

As a consequence, although the results obtained, under the same conditions, with different gases and pressures indicate this to be a true effect, it is possible that the ionic asymmetric Stark effect is still masked under the accumulation of different Stark symmetric shifts and broadenings. To obtain a definite answer, a more systematic investigation and a more detailed (time-resolved) investigation effect is worth of.
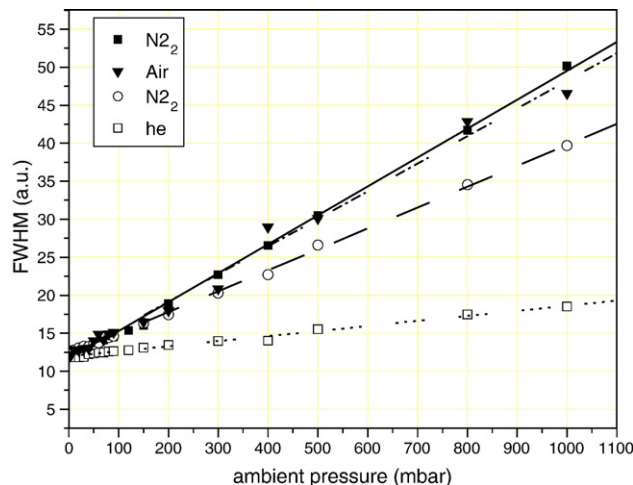

Fig. 7. FWHM of the 827.24 nm Br line as a function of the ambient gas pressure for He, O$_2$, air and N$_2$.

In the LIBS bibliography, this asymmetric Stark broadening due to ionic influence has scarcely been studied: only recently [46], the ion Stark effect on the Fe I 538.34 nm line has been observed and systematically investigated. This study employed the fundamental Nd:YAG laser at 100 mJ per pulse on a 50% Fe–Ni alloy in air. A detailed examination of the spatial variation and temporal evolution of the line profile was presented, revealing the significant contribution of the ionic influence on the shift and asymmetric broadening of this Fe I line. There are many differences between this work and ours. The ionic effect in Fe was studied (*a*) at different radial positions away from the laser focus, for a constant delay and width of the observation window and (*b*) for different temporal windows recording spatially integrated spectra. Our work presents a study of the Br line profile (*a*) integrating the plasma emission from the plasma core, from a volume according to the acceptance angle of the fiber, (*b*) in dependence on the ambient gas species (air, O_2, N_2 and He) and (*c*) in dependence on the pressure and therefore the gas density in the range from a few mbar to about 1 atm. In addition, for the first time, a UV laser wavelength produced such a degree of ionization that revealed the asymmetry in a Br emission line profile.

To the best of our knowledge, the first published indication on the effects of surrounding air pressure on shift and broadening is reported in Ref. [38], where a 337 nm N_2 laser was used to study the Cu II 254.5 nm line profile. There was some indication of an asymmetric line broadening, but no detailed reference was made to it. Very probably, the pulse energy of only 3 mJ of the laser available was not adequate to produce a higher degree of ionization and lead to a more pronounced effect.

To study in some more detail the ambient gas effects on the bromine line profile, we plotted in Fig. 7 the full width at half maximum (FWHM) of the 827.24 nm line as a function of the ambient gas pressure value. For all four gases used, a good linearity results between the FWHM and the pressure. In particular, we notice that the selection of pressure and gas is rather crucial for obtaining the optimum operating conditions, to avoid line broadening, causing line overlap in analytical applications where Br detection is required in the presence of other elements. Further, we observe that for ambient gas pressure up to 80 mbar, the broadening is comparable for all gases.

The difference in the broadening effect between the various gases stems from the different physical properties of the various gases used [41,44,47]. For an explanation in a first approximation, He is characterized by the highest ionization potential at 24.59 eV and largest thermal conductivity ($360.36 \ 10^{-6}$ cal s^{-1} deg^{-1} cm^{-1}), compared to the other gases. It is therefore less ionized and cools faster: thus it least affects the bromine line broadening. The IP values of nitrogen and oxygen (at 15.57 and 12.06 eV respectively) are significantly lower, therefore they are easier ionized and produce a stronger Stark effect in the plasma. The fact that oxygen, other than expected, based alone on its lower IP value, produces less broadening than nitrogen, might be explained by its slightly higher thermal conductivity that nitrogen. This means that within the observation window (1 μs delay and 20 μs width) O_2 has cooled down faster, therefore the Stark microfields are smaller and thus they affect less the bromine line profile. To fully examine which physical property

dominates on the line broadening effect, more ambient gases (e.g. noble gases) should be used and their impact on the line width should be systematically studied.

4. Conclusions

Efficient qualitative and quantitative determination of bromine via LIBS in the NIR has been presented in this work. An intense, interference-free 827.24 nm Br (I) line with large signal-to-noise was formed under a combination of UV (355 nm) laser wavelength, a controlled He pressure ambient environment and a gated detector. The ambient pressure, as well as gas species, have a significant effect on line strength. Various ambient environments and detailed pressure values were investigated revealing that helium under 100 mbar produces emission signal with a more than two-orders of magnitude better signal-to-noise than when air at regular pressure is used. Concentration calibration curves, based on absolute signal strength are presented that show good linearity in a dynamic range of two orders.

Under air and atmospheric gases (oxygen and nitrogen) a substantial asymmetric Stark broadening and shifting of the bromine line have been observed and their dependence of the gas pressure has been observed. This effect, however, is much less present when helium is used.

The selection of pressure and gas type is crucial for obtaining the optimum operating conditions, to avoid line broadening, causing line overlap in analytical applications where Br detection is required in the presence of other elements. For ambient gas pressure up to 80 mbar, the broadening is comparable for all gases.

Acknowledgement

References

[1] M. Hemmerlin, R. Meillanda, H. Falk, P. Wintjens, L. Paulard, Application of vacuum ultraviolet laser-induced breakdown spectrometry for steel analysis comparison with spark-optical emission spectrometry figures of merit, Spectrochim. Acta Part B 56 (2001) 661–669.

[2] C. Haisch, R. Niessner, O.I. Matveev, U. Panne, N. Omenetto, Element-specific determination of chlorine in gases by laser-induced breakdown spectroscopy LIBS, Fresenius J. Anal. Chem. 356 (1996) 21–26.

[3] R. Sattmann, I. Monch, H. Krause, R. Noll, S. Couris, A. Hatziapostolou, A. Mavromanolakis, C. Fotakis, E. Larrauri, R. Miguel, Laser-induced breakdown spectroscopy for polymer identification, Appl. Spectrosc. 52 (1998) 456–461.

[4] D.A. Cremers, L.J. Radziemski, Detection of chlorine and fluorine in air by laser-induced breakdown spectroscopy, Anal. Chem. 55 (1983) 1252–1256.

[5] L. Durange, P. Adam, J. Amouroux, Time-resolved laser-induced spectroscopy: application for qualitative and quantitative detection of fluorine, chlorine, sulfur, and carbon in air, Appl. Spectrosc. 52 (1998) 1321–1327.

[6] E.D. Lancaster, K.L. McNesby, R.G. Daniel, A.W. Miziolek, Spectroscopic analysis of fire suppressants and refrigerants by laser-induced breakdown spectroscopy, Appl. Opt. 38 (1999) 1476–1480.

[7] M. Tran, Q. Sun, B.W. Smith, J.D. Winefordner, Determination of F, Cl and Br in solid organic compounds by laser-induced plasma spectroscopy, Appl. Spectrosc. 55 (2001) 739–744.

[8] G. Wilsch, F. Weritz, D. Schaurich, H. Wiggenhauser, Determination of chloride content in concrete structures with laser-induced breakdown spectroscopy, Constr. Build. Mater. 19 (2005) 724–730.

[9] I. Radivojevic, R. Niessner, C. Haisch, S. Florek, H. Becker-Ross, U. Panne, Detection of bromine in thermoplasts from consumer electronics by laser-induced plasma spectroscopy, Spectrochim. Acta Part B 59 (2004) 335–343.

[10] A. Gonzalez, M. Ortiz, J. Campos, Determination of sulfur content in steel by laser-produced plasma atomic emission spectroscopy, Appl. Spectrosc. 49 (1995) 1632–1635.

[11] S. Kaski, H. Hakkanen, J.E.I. Korppi-Tommola, Sulfide mineral identification using laser-induced plasma spectroscopy, Miner. Eng. 16 (2003) 1239–1243.

[12] F. Weritz, S. Ryahi, D. Schaurich, A. Taffe, G. Wilsch, Quantitative determination of sulfur content in concrete with laser-induced breakdown spectroscopy, Spectrochim. Acta Part B 60 (2005) 1121–1131.

[13] D.A. Spears, A review of chlorine and bromine in some United Kingdom coals, Int. J. Coal Geol. 64 (2005) 257–265.

[14] S.V. Vassilev, G.M. Eskenazy, C.G. Vassileva, Contents, modes of occurrence and origin of chlorine and bromine in coal, Fuel 79 (2000) 903–921.

[15] J. Vehlow, F.E. Mark, Influence of bromine on metal volatilization in waste combustion, J. Mater. Cycles Waste Manag. 2 (2000) 89–99.

[16] R. Linton, P. Williams, C. Evans, J. Natusch, Determination of the surface predominance of toxic elements in airborne particles by ion microprobe mass spectrometry and auger electron spectrometry, Anal. Chem. 49 (1977) 1514–1520.

[17] M. Stepputat, R. Noll, On-line detection of heavy metals and brominated flame retardants in technical polymers with laser-induced breakdown spectrometry, Appl. Opt. 42 (2003) 6210–6220.

[18] A. Sjoedin, H. Carlsson, K. Thuresson, S. Sjoelin, A. Bergman, C. Oestman, Flame retardants in indoor air at an electronics recycling plant and at other work environments, Environ. Sci. Technol. 35 (2001) 448–454.

[19] T. Hyotylainen, K. Hartonen, Determination of brominated flame retardants in environmental samples, Trans. Anal. Chem. 21 (2002) 13–30.

[20] L.A. Barrie, J.G. den Hartog, W. Bottenheim, S. Landsberger, Anthropogenic aerosols and gases in the lower troposphere at Alert, Canada, in April 1986, J. Atmos. Chem. 9 (1989) 101–127.

[21] M. Martinez, T. Arnold, D. Perner, The role of bromine and chlorine chemistry for arctic ozone depletion events in Ny-AK lesund and comparison with model calculations, Ann. Geophys. 17 (1999) 941–956.

[22] A.P. Vinogradov, The elementary chemical composition of marine organisms, Mem. Sears Fdn mar. Res., vol. 2, 1953, p. 647.

[23] P. Saenger, A rapid spectrophotometric method for the determination of bromine in seawater and in the ash of marine algae, Helgol. Wiss. Meeresunters. 23 (1972) 32–37.

[24] G. Asimellis, S. Hamilton, A. Giannoudakos, M. Kompitsas, Controlled inert gas environment for enhanced chlorine and fluorine detection in the visible and near-infrared by laser-induced breakdown spectroscopy, Spectrochim. Acta Part B 60 (2005) 1132–1139.

[25] G. Asimellis, A. Giannoudakos, M. Kompitsas, New near-infrared LIBS detection technique for sulfur, Anal. Bioanal. Chem. 385 (2006) 333–337.

[26] S. Hamilton, E. Al-Wazzan, A. Hanvey, A. Varagnat, S. Devlin, Fully integrated wide wavelength range LIBS system with high UV efficiency and resolution, J. Anal. At. Spectrom. 19 (2004) 479–482.

[27] A. Bogaerts, Z. Chen, Effect of laser parameters on laser ablation and laser-induced plasma formation: a numerical modeling investigation, Spectrochim. Acta Part B 60 (2005) 1280–1307.

[28] J.A. Aguilera, C. Aragon, F. Penalba, Plasma shielding effect in laser ablation of metallic samples and its influence on LIBS analysis, Appl. Surf. Sci. 129 (1998) 309–314.

[29] E.H. Evans, J.B. Dawson, A. Fisher, W.J. Price, C.M.M. Smith, J.F. Tyson, Advances in atomic emission, absorption and fluorescence spectrometry and related techniques, J. Anal. At. Spectrom. 17 (2002) 622–651.

[30] O. Samek, A. Kurowski, S. Kittel, S. Kukhlevsky, R. Hergenroderk, Ultra-short laser pulse ablation using shear-force feedback: femtosecond laser induced breakdown spectroscopy feasibility study, Spectrochim. Acta Part B 60 (2005) 1225–1229.

[31] T. Efthimiopoulos, D. Dogas, I. Palli, C. Gravalidis, M. Campbell, Plasma shielding of a XeCl-laser-irradiated YBCO target, Appl. Phys., A 71 (2000) 325–329.

[32] J.P. Singh, H.S. Zhang, F.Y. Yueh, K.P. Carney, Investigation of the effects of atmospheric conditions on the quantification of metal hydrides using laser-induced breakdown spectroscopy, Appl. Spectrosc. 50 (1995) 764–773.

[33] A.R. Striganov, N.S. Sventitskii, Tables of Spectral Lines of Neutral and Ionized Atoms, Plenum press, New York, 1986.

[34] G. Asimellis, A. Giannoudakos, M. Kompitsas, Accurate wavelength calibration in the Near-InfraRed for multielement analysis without the need of reference spectra, Appl. Opt. 45 (35) (2006).

[35] I. Bassiotis, A. Diamantopoulou, A. Giannoudakos, F.R. Kalantzopoulou, M. Kompitsas, Effects of experimental parameters in quantitative analysis of steel alloy by laser-induced breakdown spectroscopy, Spectrochim. Acta Part B 56 (2001) 671–683.

[36] M.M. Suliyanti, S. Sardy, A. Kusnowo, R. Hedwig, S.N. Abdulmadjid, K.H. Kurniawan, T.J. Lie, M. Pardede, K. Kagawa, M.O. Tjia, Plasma emission induced by an Nd-YAG laser at low pressure on solid organic sample, its mechanism, and analytical application, J. Appl. Phys. 5 (2005) 053305.

[37] S.N. Abdulmadjid, M.M. Suliyanti, K.H. Kurniawan, T.J. Lie, M. Pardede, R. Hedwig, K. Kagawa, M.O. Tjia, An improved approach for hydrogen analysis in metal samples using single laser-induced gas plasma and target plasma at Helium atmospheric pressure, Appl. Phys., B 82 (2006) 161–166.

[38] M. Autin, A. Briand, P. Mauchien, J.M. Mermet, Characterization by emission spectroscopy of a laser-produced plasma from a copper target in air at atmospheric pressure, Spectrochim. Acta Part B 48 (1993) 851–862.

[39] S. Alexiou, Stark broadening of hydrogen lines in dense plasmas: analysis of recent experiments, Physical Review. E, Statistical Physics, Plasmas, Fluids, and Related Interdisciplinary Topics 71 (2005) 066403.

[40] C. Colón, A. Alonso-Medina, Application of a laser produced plasma: experimental Stark widths of single ionized lead lines, Spectrochim. Acta Part B 61 (2006) 856–863.

[41] I.B. Gornushkin, L.A. King, B.W. Smith, N. Omenetto, J.D. Winefordner, Line broadening mechanisms in the low pressure laser-induced plasma, Spectrochim. Acta Part B 54 (1999) 1207–1217.

[42] Y. Iida, Laser vaporization of solid samples into a hollow-cathode discharge for atomic emission-spectrometry, Spectrochim. Acta Part B 45 (1990) 1353–1367.

[43] H.R. Griem, M. Baranger, A.C. Kolb, G. Oertel, Stark broadening of neutral helium lines in a plasma, Phys. Rev. 125 (1962) 177–195.

[44] W. Lochte-Hotgreven, Plasma Diagnostics, North-Holland Publishing Co., Amsterdam, 1968, pp. 144, 160, 124.

[45] M. Sabsabi, P. Cielo, Quantitative analysis of aluminum alloys by laser-induced breakdown spectroscopy and plasma characterization, Appl. Spectrosc. 49 (1995) 499–507.

[46] J. Bengoechea, C. Aragon, J.A. Aguilera, Asymmetric Stark broadening of the FeI 538.34 nm emission line in a laser induced plasma, Spectrochim. Acta Part B 60 (2005) 897–904.

[47] S.L. Lui, N.H. Cheung, Resonance-enhanced laser-induced plasma spectroscopy: ambient gas effects, Spectrochim. Acta Part B 58 (2003) 1613–1623.